Concepción Heydorn, P.; Boronat Zaragoza, M.; Millan, R.; Moliner Marin, M.; Corma Canós, A. (2017). Identification of Distinct Copper Species in Cu-CHA Samples Using NO as Probe Molecule. A Combined IR Spectroscopic and DFT Study. Topics in Catalysis. 60(19-20):1653-1663. doi:10.1007/s11244-017-0844-7

Identification of distinct copper species in Cu-CHA samples using NO as probe molecule. A combined IR spectroscopic and DFT study

P. Concepción*, M. Boronat, R. Millán, M. Moliner and A. Corma*

Instituto de Tecnología Química, Universitat Politècnica de València-Consejo Superior de Investigaciones Científicas (UPV-CSIC), Av. de los Naranjos s/n, 46022 Valencia, Spain

* To whom correspondence should be addressed acorma@itq.upv.es; pconcepc@upvnet.upv.es

Abstract

Combining IR spectroscopy of NO adsorption on Copper exchanged molecular sieves with the chabazite structure, i.e. Cu-SAPO-34 and Cu-SSZ-13, and theoretical calculations, different types of copper species have been identified. On one hand, $[Cu\text{-}OH]^+$ species can be accurately distinguished, characterized by a νNO frequency at 1788-1798 cm^{-1} depending on their location in the chabazite structure (6R versus 8R) and composition (Cu-SAPO-34 versus Cu-SSZ-13). On the other hand, dimeric copper oxo $[Cu\text{-}O\text{-}Cu]^{2+}$ species have been properly identified by means of DFT modelling, that proposes a νNO stretching frequency of 1887 cm^{-1}, which has been confirmed experimentally in the Cu-SAPO-34 sample. Finally the location of isolated Cu^{2+} ions either in the 6R units or in the 8R positions of the chabazite cavity could be accurately defined according to DFT data, and validated in the experimental IR spectra with IR bands between 1907 and 1950 cm^{-1}. Regarding to Cu^+ species, IR spectroscopy of CO reveals different types of Cu^+ species as evidenced by their ability to form mono, di and try carbonyls. The unambiguous differentiation of different types of copper species is of great interest in further identification of active sites for the NH_3-SCR reaction.

Keywords: Cu-CHA, IR spectroscopy, NO, DFT modelling, SAPO-34, SSZ-13

1 Introduction

Based on issues such as the climate change, the increased energetic demand, the limited fossil fuel resources, and the serious environmental consequences due to the combustion of carbon containing products, it is strongly necessary to modify our actual economic model towards a more sustainable future. This means to optimize the efficiency of the industrial processes and to minimize the negative environmental impact of human activities. Nitrogen oxides (NO_x) are considered as one of the main air pollutants, responsible of acid rain, photochemical smog and ozone depletion, with very hazardous effect on the environment and human health. About half of total NO_x released to atmosphere are generated by transport activities, especially by diesel engines, and the stringent international regulations of NO_x emissions have prompted a lot of research to develop highly efficient catalysts for the elimination of NO_x. The selective catalytic reduction of NO_x with NH_3 (NH_3-SCR reaction) is a leading technology for the removal of NO_x from the exhaust gas of diesel vehicles. Fe and Cu ion exchanged Y, ZSM-5 and β zeolites have shown high activity and selectivity to N_2 under a wide range of temperatures and O_2 concentration. The main drawback of these medium and large pore zeolites is their low hydrothermal stability, which makes them unattractive for commercial applications [1, 2]. Recently, copper containing molecular sieves with the chabazite (CHA) framework, namely the silicoaluminate Cu-SSZ-13 and the silicoaluminophosphate Cu-SAPO-34, have grown great expectative as very promising catalysts to meet the future needs for the SCR of NO_x with NH_3, especially owing to their high activity in a large range of temperatures and their high hydrothermal stability [3-5]. Many mechanistic and characterization studies have been performed on these systems in order to determine the reaction mechanism and identify the nature of active sites [6-12]. However, the results reported in the literature are still controversial. Several studies propose that isolated mononuclear copper ions in exchange positions of the CHA framework are the active sites for the NH_3-SCR reaction, but the location of these active sites either in the six membered ring (6R) unit or in the eight membered ring (8R) of the CHA cavity, and the possibility of ion migration from the vicinity of the 8R to the 6R, are still under discussion [7-14]. Moreover, some authors propose $[Cu\text{-}OH]^+$ systems as plausible catalytically active species [6,15,16], while others suggest that dimeric copper-oxo species such as $[Cu\text{-}O\text{-}Cu]^{2+}$, or even CuO_x nanoclusters, could play a role in the reaction mechanism [17,18]. In a recent study it has been reported that

samples containing spectroscopically and chemically different Cu species show, however, similar SCR characteristics [12]. The large discrepancy found in the literature is in part due to the wide range of synthesis conditions used in these studies, where the Cu/Al and Si/Al ratios, as well as the post synthesis treatments influence the composition and catalytic properties of the final material. Thus, most catalysts contain a mixture of all proposed species, isolated Cu^{+} and Cu^{2+} cations in different positions, $[Cu\text{-}OH]^{+}$ species, $[Cu\text{-}O\text{-}Cu]^{2+}$ dimers and small CuO_x nanoclusters inside the channels or at the catalyst surface.

By using specific combinations of organic structure directing agents and gel compositions in a "one pot" synthesis procedure, Cu-SAPO-34 and Cu-SSZ-13 samples with well-defined uniform single active sites have been prepared in our group [5, 19-20], both of them showing high activity and stability in the NH_3-SCR reaction. It has been possible with this synthetic method to accurately control framework Al (in SSZ-13) or Si (in SAPO-34) distribution as well as Cu occupancy in the range 1.0 – 0.2 atoms per cavity, both of them key parameters in the hydrothermal stability of the materials. Sample characterization by conventional techniques like powder X-ray diffraction (PXRD), X-ray photoelectron spectroscopy (XPS) and Temperature Programed H_2 Reduction (H_2-TPR) have confirmed the presence of well dispersed copper cations. However, the location of these cations at specific positions in the structure, their coordination degree, and their presence as isolated, dimeric or $[Cu\text{-}OH]^{+}$ species are not yet resolved, these being critical aspects in the catalytic behavior of the final material.

Many spectroscopic techniques with high resolution have been developed which deliver precise information on the composition, topology, and local environment of active sites in solid materials, such as X-ray photoelectron spectroscopy (XPS), Auger (AES) spectroscopy, X-ray adsorption spectroscopy (XAS), surface microscopy methods, Infrared spectroscopy, Raman spectroscopy, etc. Among all these techniques, Infrared spectroscopy is a highly valuable tool because it provides relevant information about the chemical nature of adsorbed surface species, their interaction strength and geometry. However, it remains practically blind with respect to the chemical properties of the surface sites, like oxidation state, coordination environment, or Lewis acidity and/or basicity, which are decisive in the catalytic properties of the material. In this situation, information is obtained by using specific molecules, labeled probe molecules, whose vibrational frequencies are modified by interaction with the surface sites. Following by

IR spectroscopy the changes in the vibrational spectra of the probe molecules it is possible to obtain very accurate information about the chemical properties of the surface sites. In this sense, a large number of papers and reviews have been published highlighting the great potential of IR spectroscopy for surface characterization using specific probe molecules [21-30], and their impact in catalysis [31-34]. CO and NO are very good candidates for surface characterization, because they fulfil the conditions required for a probe molecule, such as small size and accordingly good accessibility to surface sites, softness, low chemical reactivity, etc. Compared to CO, NO should show a higher sensitivity to the electronic state of the cation where it coordinates, due to an unpaired electron in the NO antibonding 2π orbital. But in many cases, the use of a specific molecule depends on the intrinsic properties of the metallic site. Thus, for example, CO is more sensitive than NO in the determination of Cu^{+} species [35-42] while, in contrast, Cu^{2+} interacts weakly with CO [21,43] and NO is highly sensitive toward Cu^{2+} sites [35,44-48]. Despite the high surface sensitivity offered by IR spectroscopy, IR band assignation is in some cases a challenge due to the complexity of heterogeneous catalysts, where different sites co-exist leading to IR band overlapping and dipole-dipole effects. Moreover, and specifically in the case of NO, its high chemical reactivity even when working at low temperature (77K), makes spectra interpretation very difficult. In this case, it is possible to identify distinct surface sites with high accuracy by combining theoretical modelling of the vibrational frequencies of adsorbed probe molecules with experimental IR data [25-26, 49-52].

Taking advantage of the high sensitivity of CO and NO as IR probe molecules, and in view of the controversy existing in the literature about the nature of the catalytically active species in the NH_3-SCR reaction catalyzed by Cu-exchanged molecular sieves, the aim of this work is to identify and characterize all copper species present in the Cu-SSZ-13 and Cu-SAPO-34 samples synthesized in our group, which show a very good catalytic performance in the NH_3-SCR reaction. In the present study, we have combined IR experimental data of CO and NO adsorption with theoretical calculations, enabling an accurate assignation of the νNO vibrational frequencies, specifically in those cases where ambiguity exists in the literature. With this approach, monovalent Cu^{2+} and Cu^{+} ions located either in the 6R or 8R units of the CHA structure, $[Cu\text{-}OH]^{+}$ species and $[Cu\text{-}O\text{-}Cu]^{2+}$ dimers have been identified.

2 Experimental section

2.1 Synthesis

Cu-SAPO-34 and Cu-SSZ-13 samples were synthesized by a "one pot method" as described in detail in references [19] and [20]. Briefly, Cu-SAPO-34 sample was prepared by hydrothermal synthesis [19], with a final gel composition of: 0.29 Al_2O_3 : 0.20 P_2O_5 : 0.17 SiO_2 : 0.04 Cu-TEPA : 0.15 DEA : 0.3 TEABr : 10 H_2O. The resulting gel was heated at 150ºC under static conditions for 5 days. The crystalline product was filtered, washed and dried at 100ºC overnight. Finally it was calcined at 550ºC in air to properly remove the occluded organic species. The PXRD pattern of the solid shows the crystallization of the Cu-SAPO-34 material as pure phase, and chemical analyses reveal a Si/(Al+P) and a Cu/TO_2 molar ratios of 0.15 and 0.031 (corresponding to ~0.4 Cu atoms per cavity of CHA), respectively.

Cu-SSZ-13 sample was prepared by hydrothermal synthesis [20], with a final gel composition of: SiO_2 : 0.062 Al_2O_3 : 0.02 Cu-TEPA : 0.15 TMAdaOH : 0.2 NaOH : 20 H_2O. The resultant gel was heated at 150ºC under static conditions for 10 days. The crystalline product was filtered, washed and dried at 100ºC overnight. Finally it was calcined at 550ºC in air to remove the entrapped organic species. The PXRD pattern of the solid shows the crystallization of the Cu-SSZ-13 material as pure phase, and chemical analyses reveal a Si/Al and a Cu/TO_2 molar ratios of 8.4 and 0.019 (corresponding to ~0.2 Cu atoms per cavity of CHA), respectively.

The PXRD, TPR and XPS data of the prepared samples, as well as their catalytic performance in the NH_3-SCR reaction are given in Online Resource.

2.2 Characterization

IR spectra were recorded with a Thermo "Nexus 8700" FTIR spectrometer using a DTGS detector and acquiring at 4 cm^{-1} resolution. A homemade IR cell allowing in situ treatments in controlled atmospheres and temperatures from -176 ºC to 500 ºC was connected to a vacuum system with gas dosing facility. For IR studies the samples were pressed into self-supported wafers and activated at 350 ºC in Oxygen flow (20 ml min^{-1})

for 2 h followed by evacuation at 10^{-5} mbar at 150ºC for 1h. Vacuum treatment under these conditions is not reductive according to literature data [53]. After activation the samples were cooled down to -176ºC (for CO adsorption studies) and to -156ºC (for NO adsorption studies) under dynamic vacuum conditions followed by CO or NO dosing at increasing pressure (0.2-2mbar for CO and 0.05-0.6mbar for NO). IR spectra were recorded after each dosage. After maxima CO and NO dosing the samples were evacuated under dynamic vacuum conditions at 10^{-5}mbar and IR spectra acquired at controlled times. In another set of experiments the samples were pre-activated in vacuum (10^{-5} mbar) at 400ºC for 2h, prior to the IR study.

2.3 Computational methods

Periodic density functional calculations were performed using the Perdew-Wang (PW91) exchange-correlation functional within the generalized gradient approach (GGA) [54, 55] as implemented in the VASP code [56, 57]. The valence density was expanded in a plane wave basis set with a kinetic energy cutoff of 450 eV, and the effect of the core electrons in the valence density was taken into account by means of the projected augmented wave (PAW) formalism [58]. Integration in the reciprocal space was carried out at the Γ k-point of the Brillouin zone. Electronic energies were converged to 10^{-6} eV and geometries were optimized until forces on atoms were less than 0.015 eV/Å. The chabazite structure was modelled by means of a hexagonal unit cell with lattice parameters $a = b = 13.8026$ Å, $c = 15.0753$ Å, $\alpha = \beta = 90^{o}$ and $\gamma = 120^{o}$ containing 36 Si and 72 O atoms. The SSZ-13 model contains either 1 Al and 35 Si atoms (Si/Al ratio = 35) or 2 Al and 34 Si atoms (Si/Al ratio = 17), and the SAPO-34 model contains either 1 Si, 17 P and 18 Al ((Al+P)/Si ratio = 35) or 2 Si, 16 P and 18 Al ((Al+P)/Si ratio = 17). As shown in Scheme 1, two Al atoms in SSZ-13 can be in the same 6R ring (structures 2Al-6Ra and 2Al-6Rb) in the same D6R unit (structure 2Al-D6R) or in the same 8R ring (structure 2Al-8R). In the case of SAPO-34, only the corresponding 2Si-6Rb, 2Si-D6R and 2Si-8R can exist. For each possible distribution, Cu^{+}, Cu^{2+}, $[Cu(OH)]^{+}$ and $[Cu\text{-}O\text{-}Cu]^{2+}$ species were placed in the 6-membered rings (6R) or in the 8-membered rings (8R) of the chabazite structure compensating the negative charges generated by isomorphic substitution in the framework. The optimized structures of all models considered and their relative stability are shown in Online Resource 1. The interaction of NO with Cu^{+}, Cu^{2+}, $[Cu(OH)]^{+}$ and $[Cu\text{-}O\text{-}Cu]^{+}$ species was investigated by placing one or two NO molecules close to the copper species and

optimizing the geometry of the whole system. Finally, vibrational frequencies were calculated by diagonalizing the block Hessian matrix corresponding to displacements of the Cu, N, H and O atoms not belonging to the catalyst framework.

It should be noted here that, as clearly described by Göltl et al. [52,59] an accurate simulation of the IR spectra for every particular copper site would require the use of molecular dynamics simulations and the consideration of all stable local Al distributions and Cu siting. However, it has also been demonstrated that static GGA calculations provide reliable NO stretching frequencies that can be used to assist in the assignation of experimentally observed IR bands, this being the approach employed in this study [51,60, 61].

3 Results

The presence of isolated copper species, predominately in a Cu^{2+} oxidation state, was confirmed by H_2-TPR and XPS studies (see online resource) on both Cu-SAPO-34 and Cu-SSZ-13 samples, where small amounts of dispersed copper oxide nanoclusters could also be detected in the Cu-SAPO-34 sample. Small amount of Cu^{+} was observed on both samples. Thus, in order to gain information about the nature of both Cu^{2+} and Cu^{+} species, IR spectroscopy of CO adsorption was performed for a specific analysis of Cu^{+} species while NO adsorption studies were mainly directed toward the study of Cu^{2+} species. In addition to the copper containing samples, i.e Cu-SAPO-34 and Cu-SSZ-13, copper free samples were also considered and discussed. The assignation of the IR bands associated to Cu-CO complexes was done based on literature data due to a general agreement in the interpretation of their vibrational spectra. However, in the case of Cu-NO complexes, and due to the ambiguity found in the literature data, assignation of the IR bands was mainly done in combination with theoretical DFT calculations.

3.1. IR spectroscopy of adsorbed CO

CO has been reported as a very sensitive probe molecule for studying unsaturated Cu^{+} species [35-42, 52], while it remains insensitive toward Cu^{2+}. Depending on the local environment of Cu^{+} ions, their coordination degree, steric and electronic effects mono-, bi- and tri-coordinated carbonyl complexes can be stabilized. In addition, CO can

interact with other Lewis acid sites (like for example extra-framework Al^{3+}) and with OH groups present in the catalysts, giving in the last case valuable information about their Brönsted acid properties.

Interaction of CO with Cu-SSZ-13.

Fig.1 shows the IR spectra of CO adsorption on the Cu-SSZ-13 and the copper free SSZ-13 zeolites at increasing CO dosing. The Infrared OH region is shown in fig.1a and the corresponding CO region is shown in fig.1b.

As shown in Fig.1b, two IR bands at 2158 cm^{-1} and 2136 cm^{-1} are observed in the IR spectra of the Cu-SSZ-13 zeolite at low CO dosing, while no associated shift in the bands corresponding to OH groups is appreciated in Fig.1a. The IR band at 2158 cm^{-1} has been attributed to mono-carbonyl Cu^{+}(CO) complexes associated to Cu^{+} ions in ion exchange zeolite positions [21,62,], while the IR band at 2136 cm^{-1} has been more discussed. Whereas in some cases it has been ascribed to Cu^{+} ions on the surface of bulk copper oxide or on highly dispersed Cu_2O nanoclusters present in copper exchanged zeolites [21,63], other authors have assigned a similar IR band to Cu^{+} ions located in constrained environments of the SSZ-13 structure [12,62] or in a specific location in the 6R [52]. Moreover co-adsorption of ligands (like methanol or dimethyl ether) to the Cu^{+}-CO species has been reported to shift its IR frequency to lower values (from 2155 cm^{-1} to 2129 and 2133 cm^{-1}) [64], suggesting one possible assignation of the 2136 cm^{-1} IR band to a copper species where CO and OH are co-adsorbed. When increasing CO dosing, a shift of the bands corresponding to hydroxyl groups is clearly observed in the OH region (Fig.1a) with a gradual depletion of the 3612, 3579 and 3531 cm^{-1} IR bands and the parallel appearance of two new bands at 3315 and 3458 cm^{-1}. Similar behavior is also observed on the copper free SSZ-13 sample, and compares well with recent studies [65]. The IR bands at 3612 and 3579 cm^{-1} have been associated to Brönsted acid sites of similar acid strength, red shifted to 3315 cm^{-1} due to OH-CO interaction, while the 3531 cm^{-1} band is due to silanol groups shifted to 3458 cm^{-1} by the CO interaction. In the νCO region (Fig.1b), the OH-CO interaction is characterized by an IR band at 2177cm^{-1}, as clearly stated from the copper free sample. At increasing CO dosing, in addition to the growing of the aforementioned IR band, a shoulder appears at 2148 cm^{-1} in the Cu-SSZ-13 sample which has been ascribed to the asymmetric stretching modes

of a di-carbonyl $Cu^{+}(CO)_2$ complex [21,62]. Their symmetric mode at 2177cm^{-1} is overlapped by the strong CO-OH band.

Interaction of CO with Cu-SAPO-34

The interaction of CO with Cu-SAPO-34 and copper free SAPO-34 samples is shown in Fig.2, in the OH region (Fig.2a) and in the CO frequency region (Fig.2b).

At low CO dosing, CO interacts only with copper ions in the Cu-SAPO-34 sample, since no shift in the OH groups is observed (Fig.2a). IR bands at 2139, 2163, 2187 cm^{-1}; 2147, 2178 cm^{-1}; and 2154 cm^{-1}, associated to tri-carbonyl $Cu^{+}(CO)_3$, di-carbonyl $Cu^{+}(CO)_2$ and mono-carbonyl Cu^{+}-CO complexes respectively, are observed (Fig.2b), in addition to another signal at 2131cm^{-1}. Based on the TPR data (see online resource), and despite the ambiguity found in the literature in the assignation of the 2131cm^{-1} IR band (see discussion above), it is possible to assign the 2131cm^{-1} IR band to small amounts of Cu oxide nanoclusters present in the Cu-SAPO-34 sample. At increasing CO dosing the intensity of all bands increases, in addition to the growing of an IR band at 2171cm^{-1}, and the appearance of new bands at 2220 cm^{-1} and ~ 2205 cm^{-1}. The IR band at 2171cm^{-1} is due to CO interacting with OH groups, as clearly evidenced from the IR spectra of CO adsorption on the copper free sample, and the bands at 2220 and 2205 cm^{-1} can been ascribed to different types of extra framework Al^{3+} species [66]. Meanwhile, in a recent study [62] the band at 2205 cm^{-1} has been associated to $[Cu\text{-}OH]^{+}$ species interacting with CO, supported by the presence of a 3660 cm^{-1} IR band in the ν(OH) region [56, JACS]. In the OH region (Fig.2a), a gradual shift in the Cu-SAPO-34 hydroxyl groups is observed at increasing CO coverages, with a gradual depletion of the IR bands associated to Brönsted acid sites at 3622 and 3595 cm^{-1} and the appearance of a new IR band at c.a. 3369 cm^{-1}, while no IR band at ~3660cm^{-1} is detected. Notice a lower OH shift in the Cu-SAPO-34 sample compared to the Cu-SSZ-13 sample, corresponding to a lower Brönsted acidity. Similar trend in acidity have been observed in the copper free samples, and agrees with literature data [65].

In summary, a slight different nature of Cu^{+} ions has been evidenced in both samples, where mono- and di-carbonyl species are stabilized in the Cu-SSZ-13 sample while mono-, di- and tri-carbonyl species are present in the Cu-SAPO-34 sample.

3.2. IR spectroscopy of adsorbed NO

While CO is a valuable probe molecule to characterize Cu^{+} species, NO has been shown to be highly sensitive toward Cu^{2+}, giving characteristic IR bands in the 1950–1870 cm^{-1} IR region. Moreover, NO can also interact with Cu^{+} species, leading to the appearance of IR bands in the 1850–1700 cm^{-1} region, and with surface hydroxyl groups. Altogether, using NO as probe molecule in IR studies, detailed information of all the species present in Cu-SSZ-13 and Cu-SAPO-34 catalysts, including Cu^{+}, Cu^{2+} and acid sites, can be obtained.

Interaction of NO with Cu-SSZ-13

The IR spectra of NO adsorbed on Cu-SSZ-13 and on copper free SSZ-13 samples are shown in Fig.3, with the OH region shown in Fig. 3a and the corresponding NO region in Fig. 3b. Notice the presence of an IR band at 1894 cm^{-1} observed in the NO frequency region of the IR spectra of the copper free SSZ-13 zeolite (Fig. 3b). A parallel shift in the bands present in the OH region of SSZ-13 (Fig. 3a) indicates that the IR band at 1894 cm^{-1} is associated to NO interacting with hydroxyl groups. At increasing NO coverages, several new IR bands appear in the spectrum of SSZ-13 sample, at 1870, 1823 and 1769 cm^{-1}, which may correspond to physisorbed $(NO)_2$ (1870 and 1769 cm^{-1}) [22] and other NO adducts not related to copper species (1823 cm^{-1}), which may arise due to the high reactivity of NO.

In the Cu-SSZ-13 sample, the IR spectra of NO adsorption at low NO dosing shows several IR bands with maxima at c.a.1950, 1924, 1909, and 1896 cm^{-1} in the NO frequency region (Fig.3b), in parallel to a shift in the OH groups (Fig. 3a). At increasing NO dosing, an increase in the intensity of the previous bands is observed, as well as the growing of new IR bands in the low frequency region, i.e at 1870, 1827, 1802-1788, 1729 and 1698 cm^{-1}. In view of the spectra obtained for the SSZ-13 sample, IR bands at 1950, 1924 and 1909 cm^{-1}, and those arising at low NO dosing in the low frequency range, i.e 1827, 1802-1788, 1729 and 1698 cm^{-1} can be assigned to Cu-NO adducts. Caution has to be taken in the analysis of the IR peaks in the low frequency range, where the undiscriminating increase in the intensity of the IR bands at 1827 and 1729 cm^{-1}, is related to the formation of NO adducts not associated to copper species. The precise assignation of all these bands to particular copper species requires the assistance of DFT modeling, as described in the Discussion section.

Interaction of NO with Cu-SAPO-34

The IR spectrum of NO adsorbed on the copper free SAPO-34 at low NO dosing (Fig. 4b) is quite similar to that described for SSZ-13, and shows the interaction of NO with hydroxyl groups, characterized by an IR band at 1892 cm^{-1}. At increasing NO dosing new bands at 1870 and 1762 cm^{-1} appear, related to physisorbed $(NO)_2$. The IR spectrum of the Cu-SAPO-34 sample at low NO dosing is also similar to that of Cu-SSZ13, with bands at 1943, 1924 and 1911 cm^{-1} that can be safely assigned to Cu-NO adducts. But at increasing NO dosing, a new intense IR band appears at 1883 cm^{-1} together with other signals at 1820 and 1753 cm^{-1} (Fig.4b). In particular, the band at 1883 cm^{-1}, which to our knowledge is not referenced in the literature, remains quite stable under evacuation, and it is strongly dependent on the pre-activation conditions of the sample. Indeed, when the Cu-SAPO-34 sample is activated in vacuum at 400ºC (reducing conditions), the 1883cm^{-1} IR is not present any more, or it is in very low amount (Fig.5). As indicated above, the intensity grow of the 1753cm^{-1} IR band at increasing NO dosing is related to NO adducts not associated to Cu species, assisted by the high reactivity of NO.

In the OH region of the CuSAPO-34 sample, a shift in the hydroxyl groups (i.e IR bands at 3622, 3595 and 3536 cm^{-1}) is observed at increasing NO dosing, together with the growing of new bands at 3465 and 3381cm^{-1} (Fig.4a).

3.3. Theoretical calculations

While there exists agreement in the literature regarding IR band assignation of CO interacting with copper sites, that is not the case for NO. Thus, in order to assist in the assignation of the bands in the IR spectra of NO adsorption, the interaction of one and two NO molecules with different models of Cu^{+}, Cu^{2+}, $[Cu(OH)]^{+}$ and $[Cu\text{-}O\text{-}Cu]^{2+}$ species in Cu-SSZ-13 and Cu-SAPO-34 catalysts was modelled by means of DFT calculations. The optimized structures of NO interacting with Cu^{+}, $[Cu(OH)]^{+}$ and Cu^{2+} species in Cu-SSZ-13 zeolite are depicted in Fig. 6 and Fig.7, the interaction of NO with a $[Cu\text{-}O\text{-}Cu]^{2+}$ dimer in Cu-SAPO-34 is depicted in Fig. 8, and the calculated νNO vibrational frequencies for all systems in Cu-SSZ-13 and Cu-SAPO-34 are summarized in Table 1.

NO interacts strongly with all copper species modelled in this study, with calculated adsorption energies ranging from -20 to -46 kcal/mol depending on the oxidation state and location of the copper centre. As generally agreed, νNO vibrational frequencies associated to isolated Cu^{+} species appear in the 1700–1850 cm^{-1} range, while those corresponding to NO adsorbed on Cu^{2+} cations are shifted to higher frequencies. Thus, the calculated frequencies for mono-nitrosyl $Cu^{+}(NO)$ complexes in Cu-SSZ-13 and Cu-SAPO-34 are between 1805 and 1820 $cm^{-1.}$ For di-nitrosyl $Cu^{+}(NO)_2$ complexes, the asymmetric stretching modes appear at lower frequencies, ~ 1660 cm^{-1} in Cu-SSZ-13 and at ~ 1720 cm^{-1} in Cu-SAPO-34, while the calculated frequencies for the symmetric modes are similar or slightly larger than those corresponding to mono-nitrosyl systems. These calculated frequencies match the experimental data obtained for Cu-SSZ-13 sample at low NO dosing with IR bands at 1827 and 1698 cm^{-1} and for Cu-SAPO-34 with IR bands at 1820 and 1753 cm^{-1}, corresponding to mono and di-nitrosyl complexes in both 6R and 8R environments. On the other hand, the interaction of NO with $[Cu(OH)]^{+}$ species is strong, and results in calculated vibrational frequencies between 1787 and 1798 cm^{-1}. An IR band at 1788 cm^{-1} is clearly detected in the Cu-SSZ-13 sample (Fig.3b). Moreover, based on this assignation, we can attribute the 2136cm^{-1} IR-CO band in Fig.1b to the same $[Cu(OH)]^{+}$ species. This result is supported by an IR band at 3668 cm^{-1} due to the hydroxyl group (see online resource). The interaction of NO with Brönsted acid sites, on the contrary, is weak, and the corresponding νNO vibrational frequencies are 1891 cm^{-1} in both materials, in good agreement with the experimental data.

NO adsorption on isolated Cu^{2+} cations was also considered, and vibrational frequencies between 1925 and 1977 cm^{-1} were obtained on Cu-SSZ-13 zeolite, and quite similar values between 1907 and 1968 cm^{-1} on Cu-SAPO-34. As depicted in Fig. 7, the strong coordination of Cu^{2+} cation with three framework oxygen atoms when it is located either in the 6Rb-6R or in the 8R-8R positions makes difficult the coordination of two NO molecules, and therefore only mono-nitrosyl complexes were obtained for these two systems. The calculated νNO frequencies corresponding to mono-nitrosyl complexes in CuII-6Rb and CuII-8R-8R positions in Cu-SSZ-13, 1925 and 1947 cm^{-1}, are clearly observed in the experimental spectrum of NO adsorption with IR bands at 1924 and 1950 cm^{-1} (Fig. 3b). And the same occurs in Cu-SAPO-34, with calculated νNO

frequencies at 1907 and 1940 cm^{-1} and experimental values at 1911 and 1943 cm^{-1} (Fig. 4b), being associated to NO bonded to CuII-8R-8R and CuII-6Rb systems, respectively.

Finally, the interaction of NO with dimeric $[Cu\text{-}O\text{-}Cu]^{2+}$ species in Cu-SAPO-34, modelled by the structure depicted in Figure 8, left, was also investigated. Notice that the two Cu^{2+} cations belonging to the dimer are stabilized by interaction with the negative charges generated by two Si atoms placed in different 6R units, so that the $[Cu\text{-}O\text{-}Cu]^{2+}$ unit is placed across the cavity. Other possible locations of the $[Cu\text{-}O\text{-}Cu]^{2+}$ dimer were explored and found between 5 and 25 kcal/mol less stable. Adsorption of two NO molecules on the two Cu atoms of the dimer yields, after full geometry optimization, the structure depicted in Fig. 8, right. One of the NO molecules is adsorbed in a bridge mode interacting with both Cu and O atoms, and the corresponding νNO calculated vibrational frequency is 1712 cm^{-1}. The other NO molecule is bonded to the Cu atom directly attached to two O atoms in a linear configuration, a structure which is difficult to obtain in the case of isolated Cu^{2+} cations, and the corresponding calculated νNO vibrational frequency is 1887 cm^{-1}. Based on this results, it is possible to assign the band observed at 1883 cm^{-1} in the IR spectra of CuSAPO-34 to dimeric $[Cu\text{-}O\text{-}Cu]^{2+}$ species.

4. Discussion

As indicated in the introduction, unambiguous identification of the copper species present in Cu-exchanged molecular sieves is of great interest, especially since the last developments in the synthesis of highly active and hydrothermally stable copper-based catalysts for the NH_3-SCR reaction. A number of different species have been proposed as possible active sites in the aforementioned reaction, including isolated Cu^{+} and Cu^{2+} cations in non-equivalent positions and local environment in the zeolite framework, hydroxylated $[Cu\text{-}OH]^{+}$ species, $[Cu\text{-}O\text{-}Cu]^{2+}$ dimers and small CuO_x nanoclusters inside the channels or at the external surface. However specific identification of those sites is still missing. IR spectroscopy of probe molecules like CO and NO is a very useful tool to characterize the nature of the active centers in solid catalysts, due to their high sensitivity to the chemical properties of the sites on which they interact. But assignation of the IR bands is not always easy, and can lead to erroneous interpretation. By combining IR spectroscopy of CO and NO adsorption with DFT calculations it has

been possible to assign accurately to a defined state of copper species the different IR bands experimentally observed in the NO-IR spectra of Cu-SSZ-13 and Cu-SAPO-34 catalysts.

On one hand, NO adsorption followed by IR spectroscopy has allowed to unambiguously identify [Cu-OH]+ species, which are characterized by an IR band at ~ 1788- 1798 cm^{-1} depending on their location (6R versus 8R) and zeolite type (Cu-SAPO-34 versus Cu-SSZ-13). This result doesn't match a previous assignation of an IR band at 1897 cm^{-1} to NO interacting with $[Cu\text{-}OH]^{+}$ species [62, 67]. In opposite, comparison of the IR spectra of NO adsorption on Cu-SSZ-13 and Cu-SAPO-34 samples with the corresponding spectra on copper free SSZ-13 and SAPO-34 samples, together with DFT modelling, clearly shows that the IR band at ~ 1897-1894 cm^{-1} can be safely assigned to NO interacting with hydroxyl groups.

On the other hand, dimeric copper oxo $[Cu\text{-}O\text{-}Cu]^{2+}$ species have been properly identified by means of DFT modelling, that proposes a νNO stretching frequency of 1887 cm^{-1} for NO strongly bonded to Cu atoms in a particular arrangement not possible in isolated Cu^{2+} cations. Indeed, a highly stable IR band at 1882 cm^{-1}, not previously assigned in the literature, has been experimentally observed in the Cu-SAPO-34 sample after NO adsorption. Moreover, it has been shown that the intensity of the IR band associated to $[Cu\text{-}O\text{-}Cu]^{2+}$ species depends on the sample pre-activation conditions, clearly decreasing under reducing conditions.

Finally, the location of isolated Cu^{2+} ions either in the 6R units or in the 8R positions could be precisely defined according to DFT data. The good correlation found between calculated frequencies and experimental values validates the proposals from the theoretical study.

In definitive, using NO as a probe molecule and combining IR studies with DFT calculations, monovalent isolated Cu^{2+} or Cu^{+} ions located either in 6R or 8R positions within the CHA structure, $[Cu\text{-}OH]^{+}$ species, and $[Cu\text{-}O\text{-}Cu]^{2+}$ dimers can be distinctly identified, which is of great interest in the identification of active sites for the NH_3-SCR reaction.

Acknowledgments

This work has been supported by the Spanish Government through “Severo Ochoa Program” (SEV 2012-0267), and MAT2015-71261-R, the European Union through ERC-AdG-2014-671093 (SynCatMatch); and the Generalitat Valenciana through the Prometeo program (PROMETEOII/2013/011). R.M. acknowledges “La Caixa - Severo Ochoa” International PhD Fellowships (call 2015).

References

1. Wilken N, Wijayanti K, Kamasamudram K, Currier NW, Vedaiyan R, Yezerets A, Olsson L (2012) Appl. Catal. B 111:58-66
2. Kwak JH, Tran D, Burton SD, Szanyi J, Lee JH, Peden CHF (2012) J. Catal. 287:203-209
3. Kwak JH, Tonkyn RG, Kim DH, Szanyi J, Peden CHF (2010) J. Catal. 275:187-190
4. Bull I, Boorse RS, Jaglowski WM, Koermer GS, Moini A, Patchett JA, Xue WM, Burk P, Dettling JC, Caudle MT (2008) U.S. Patent 0,226,545
5. Martínez-Franco R, Moliner M, Franch C, Kustov A, Corma A (2012) Appl. Catal. B 127:273-280
6. Borfecchia E, Lomachenko KA, Giordanino F, Falsig H, Beato P, Soldatov AV, Bordiga S, Lamberti C (2015) Chem. Sci. 6:548-563
7. Beale AM, Gao F, Lezcano-Gonzalez I, Peden CHF, Szanyi J (2015) Chem. Soc. Rev. 44:7371-7405
8. Beale AM, Gao F, Lezcano-Gonzalez I, Slawinksi WA, Wragg DS (2016) Chem. Commun. 52:6170-6173
9. Kwak JH, Varga T, Peden CHF, Gao F, Hanson JC, Szanyi J (2014) J. Catal. 314:83-9
10. Korhonen ST, Fickel DW, Lobo RF, Weckhuysen BM, Beale AM (2011) Chem. Commun. 47:800-802
11. Kwak JH, Zhu H, Lee JH, Peden CHF, Szanyi J (2012) Chem. Commun. 48:4758-4760
12. Paolucci C, Parekh AA, Khurana I, Iorio JRD, Li H, Caballero JDA, Shih AJ, Anggara T, Delgass WN, Miller JT, Ribeiro FH, Gounder R, Schneider WF (2016) J. Am. Chem. Soc. 138: 6028-6048
13. Fickel DW, Fedeyko JM, Lobo RF (2010) J. Phys. Chem. C 114:1633-1640
14. Gao F, Walter ED, Karp EM, Luo J, Tonkyn RG, Kwak JH, Szanyi J, Peden CHF (2013) J. Catal. 300:20-29
15. Andersen CW, Bremholm M, Vennestrom PNR, Blichfeld AB, Lundegaard LF, Iversen BB (2014) IUCRJ 1:382-386
16. Godikse A, Stappen FN, Vennestrom PNR, Giordanino F, Rasmussen SB, Lundegaard LF, Mossin S (2014) J. Phys. Chem. C 118:23126-23138
17. Lei GD, Adelman BJ, Sárkány J, Sachtler WMH (1995) Appl. Catal. B 5:245-256

18. Da Costa P, Moden B, Meitzner GD, Lee DK, Iglesia E (2002) Phys. Chem. Chem. Phys 4:4590-4601
19. Martínez-Franco R, Moliner M, Concepcion P, Thogersen JR, Corma A (2014) J. Catal. 314:73-82
20. Martínez-Franco R, Moliner M, Thogersen JR, Corma A (2013) Chem. Cat. Chem 5:3316-3323
21. Hadjiivanov K, Vayssilov GN (2002) Adv. Catal. 47:307-511
22. Hadjiivanov K (2000) Catal Rev-Sci Eng 42:71-144
23. Zaki MI, Knözinger H (1987) Mater. Chem. Phys. 17:201-215
24. Zaki MI, Knözinger H (1987) Spectrochim. Acta 43A:1455-1459
25. Neyman KM, Strodel P, Ruzankin SP, Schlensog N, Knözinger H, Rösch N (1995) Catal. Lett. 31:273-285
26. Strodel P, Neyman KM, Knözinger H, Rösch N (1995) Chem. Phys. Letters 240:547-552
27. Spielbauer D, Mekheimer GAH, Zaki MI, Knözinger H (1996) Catal. Lett. 40:71-79
28. Hadjiivanov K, Busca G (1994) Langmuir 10:4534-4541
29. Hadjiivanov K, Lamotte J, Lavalley JC (1997) Langmuir 13:3374-3382
30. Concepción P, Hadjiivanov K, Knözinger H (1999) J. Catal. 184(1):172-179
31. Lange FC, Schmelz H, Knözinger H (1996) Appl. Catal. B 8:245-265
32. Wang D, Zhang L, Kamasamudram K, Epling WS (2013) ACS. Catal. 3:871-88
33. Combita D, Concepción P, Corma A (2014) J. Catal. 311:339-349
34. Concepción P, Botella P, López Nieto JM (2004) Appl. Catal. A 278:45-56
35. Lamberti C, Bordiga S, Salvalaggio M, Spoto G, Zecchina A, Geobaldo F, Vlaic G, Bellatreccia M (1997) J. Phys. Chem. B 101:344-360
36. Lamberti C, Palomino GT, Bordiga S, Berlier G, Acapito FD, Zecchina A (2000) Angew. Chem. Int. Ed. 39:2138-214
37. Palomino GT, Bordiga S, Zecchina A, Marra GL, Lamberti C (2000) J. Phys. Chem. B 104:8641-8651
38. Zecchina A, Bordiga S, Salvalaggio M, Spoto G, Scarano D, Lamberti C (1998) J. Catal. 173:540-542
39. Zecchina A, Bordiga S, Palomino GT, Scarano D, Lamberti C, Salvalaggio M (1999) J. Phys. Chem. B 103:3833-3844
40. Lamberti C, Bordiga S, Zecchina A, Salvalaggio M, Geobaldo F, Arean CO (1998) J. Chem. Soc. Faraday Trans 94:1519-1525
41. Palomino GT, Giamello E, Fisicaro P, Bordiga S, Lamberti C, Zecchina A (2000) Stud. Surf. Sci. Catal. 130:2915-2920
42. Xamena F, Fisicaro P, Berlier G, Zecchina A, Palomino GT, Prestipino C, Bordiga S, Giamello E, Lamberti C (2003) J. Phys. Chem. B 107:7036-7044
43. Prestipino C, Regli L, Vitillo JG, Bonino F, Damin A, Lamberti C, Zecchina A, Solari PL, Kongshaug KO, Bordiga S (2006) Chem. Mater. 18:1337-1346
44. Lamberti C, Groppo E, Spoto G, Bordiga S, Zecchina A (2007) Adv. Catal. 51:1-74
45. Lamberti C, Zecchina A, Groppo E, Bordiga S (2010) Chem. Soc. Rev. 39:4951-5001
46. Spoto G, Zecchina A, Bordiga S, Ricchiardi G, Martra G, Leofanti G, Petrini G (1994) Appl. Catal. B 3:151-172
47. Prestipino C, Berlier G, Xamena F, Spoto G, Bordiga S, Zecchina A, Palomino GT, Yamamoto T, Lamberti C (2002) Chem. Phys. Lett. 363:389-396

48. Leofanti G, Marsella A, Cremaschi B, Garilli M, Zecchina A, Spoto G, Bordiga S, Fisicaro P, Berlier G, Prestipino C, Casali G, Lamberti C (2001) J. Catal. 202:279-295
49. Boronat M, Concepción P, Corma A (2009) J. Phys. Chem. C 113:16772-16784
50. Boronat M, Concepción P, Corma A, Renz M, Valencia S (2005) J. Catal. 234:111-118
51. Zhang R, McEwen JS, Kollar M, Gao F, Wang Y, Szanyi J, Peden CHF (2014) ACS Catal.4: 4093-4105
52. Göltl F, Bulo RE, Hafner J, Sautet P (2013) J. Phys. Chem. Lett. 4: 2244-2249
53. Palomino GT, Fisicarro P, Bordiga S, Zecchina A, Giamello E, Lamberti C (2000) J. Phys. Chem. B 104:4064-4073
54. Perdew JP, Chevary JA, Vosko SH, Jackson KA, Pederson MR, Singh DJ, Fiolhais C (1992) Phys. Rev. B 46: 6671–6687
55. Perdew JP, WangY (1992) Phys. Rev. B 45: 13244–13249
56. Kresse G, Furthmüller J (1996) Phys. Rev. B 54: 11169–11186
57. Kresse G, Hafner J (1993) Phys. Rev. B *47*: 558–561
58. Blöchl PE, (1994) Phys. Rev. B 50: 17953–17979
59. Göltl F, Sautet P, Hermans I (2015) Angew. Chem. Int. Ed. 54: 7799-7804
60. Uzunova EL, Göltl F, Kresse G, Hafner J (2009) J. Phys. Chem. C 113: 5247
61. Göltl F, Hafner J, J. Chem. Phys. (2012) 136: 064503-064531
62. Giordanino F, Vennestrom PNR, Lundegaard LF, Stappen FN, Mossin S, Beato P, Bordiga S, Lamberti C (2013) Dalton Trans 42:12741-12761
63. Bordiga S, Regli L, Cocina D, Lamberti C, Bjorgen M, Lillerud KP (2005) J. Phys. Chem. B 109: 2779-2784
64. Blasco T, Boronat M, Concepción P, Corma A, Law D, Vidal-Moya JA (2007) Angew. Chem. Int. Ed 46: 3938-3941
65. Kondo JN, Nishitani R, Yoda E, Yokoi T, Tatsumi T, Domen K (2010) Phys. Chem. Chem. Phys.12: 11576-11586
66. Martens JA, Jacobs PA (2001) Stud. Surf. Sci. Catal. 137: 633-671
67. Dedecek J, Sobalík Z, Tvaruzková Z, Kaucký D, Wichterlová B (1995) J. Phys. Chem. 99: 16327-16337

Table 1. Calculated νNO vibrational frequencies (in cm^{-1}) for NO interacting with different models of Cu^{+}, $[Cu(OH)]^{+}$ and Cu^{2+} species and Brönsted acid sites in Cu-SSZ-13 and Cu-SAPO-34 catalysts, and with a $[Cu\text{-}O\text{-}Cu]^{2+}$ dimer in Cu-SAPO-34.

	CuSSZ-13		CuSAPO-34	
Model	NO	2NO	NO	2NO
CuI-6R	1803	1663, 1800	1811	1720, 1831
CuI-8R	1816	1654, 1783	1821	1714, 1828
CuII-OH-6R	1795	-	1790	-
CuII-OH-8R	1788	-	1798	-
H Brönsted	1891	-	1891	-
CuII-6Ra	1965	1801, 1892	-	-
CuII-6Rb	1925	-	1940	-
CuII-D6R	1960	1801, 1869	1968	1809, 1888
CuII-8R-6R	1977	1813, 1874	1943	1802, 1868
CuII-8R-8R	1947	-	1907	-
$[Cu\text{-}O\text{-}Cu]^{2+}$	-	-		1712, 1887

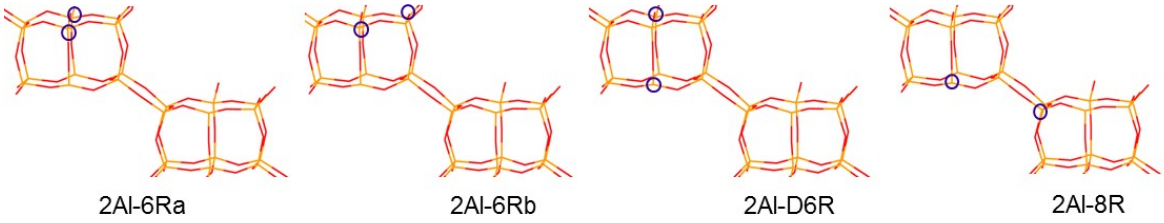

Scheme 1. Possible Al or Si distributions in SSZ-13 or SAPO-34 materials.

Figure Captions

Fig.1 IR spectra in the νOH IR region (a) and νCO IR region (b) of CO adsorption at -176ºC and at increasing CO dosing (0.2-2mbar) on the CuSSZ-13 (red) and the SSZ-13(blue) samples. The samples have been activated at 350 ºC in Oxygen flow (20 ml min^{-1}) for 2 h followed by evacuation at 10^{-5} mbar at 150ºC for 1h.

Fig.2 IR spectra in the νOH IR region (a) and νCO IR region (b) of CO adsorption at -176ºC and at increasing CO dosing (0.2-2mbar) on the CuSAPO-34 (red) and the SAPO-34 (blue) samples. The samples have been activated at 350 ºC in Oxygen flow (20 ml min^{-1}) for 2 h followed by evacuation at 10^{-5} mbar at 150ºC for 1h

Fig.3 IR spectra in the νOH IR region (a) and νNO IR region (b) of NO adsorption at -156ºC and at increasing NO dosing (0.05-0.6mbar) on the CuSSZ-13 (red) and the SSZ-13(blue) samples. The samples have been activated at 350 ºC in Oxygen flow (20 ml min^{-1}) for 2 h followed by evacuation at 10^{-5} mbar at 150ºC for 1h

Fig.4 IR spectra in the νOH IR region (a) and νNO IR region (b) of NO adsorption at -156ºC and at increasing NO dosing (0.05-0.6mbar) on the CuSAPO-34 (red) and the SAPO-34(blue) samples. The samples have been activated at 350 ºC in Oxygen flow (20 ml min^{-1}) for 2 h followed by evacuation at 10^{-5} mbar at 150ºC for 1h

Fig.5 IR spectra in the νNO IR region of NO adsorption at -156ºC and at 0.6mbar on the CuSAPO-34 sample, activated in O_2 flow at 350ºC (red) and in vacuum conditions at 400ºC (blue).

Fig. 6 Optimized geometries of NO interacting with Cu^+ and $[Cu(OH)]^+$ species in Cu-SSZ-13. Silicon, Aluminium, Oxygen, Copper, Nitrogen and Hydrogen atoms are depicted as beige, blue, red, green, purple and white balls, respectively.

Fig.7 Optimized geometries of NO interacting with Cu^{2+} species in Cu-SSZ-13. Silicon, Aluminium, Oxygen, Copper, Nitrogen and Hydrogen atoms are depicted as beige, blue, red, green, purple and white balls, respectively.

Fig. 8 Optimized geometries of a $[Cu\text{-}O\text{-}Cu]^{2+}$ dimer in Cu-SAPO-34 (left) and of two NO molecules interacting with such Cu^{2+} $[Cu\text{-}O\text{-}Cu]^{2+}$ dimer in Cu-SAPO-34 (right). Silicon, Aluminium, Phosphorus, Oxygen, Copper, Nitrogen and Hydrogen atoms are depicted as beige, blue, yellow, red, green, purple and white balls, respectively.